

# Simultaneous Source Separation, Synchronization, Localization and Mapping for 6G Systems

Alexander Venus, *Member, IEEE*, Erik Leitinger, *Member, IEEE*, and Klaus Witrisal, *Member, IEEE*  
Institute of Comm. Networks and Satellite Comms., Graz University of Technology, Austria

**Abstract**—Multipath-based simultaneous localization and mapping (MP-SLAM) is a promising approach for future 6G networks to jointly estimate the positions of transmitters and receivers together with the propagation environment. In cooperative MP-SLAM, information collected by multiple mobile terminals (MTs) is fused to enhance accuracy and robustness. Existing methods, however, typically assume perfectly synchronized base stations (BSs) and orthogonal transmission sequences, rendering inter-BS interference at the MTs negligible. In this work, we relax these assumptions and address simultaneous source separation, synchronization, and mapping. A relevant example arises in modern 5G systems, where BSs employ muting patterns to mitigate interference, yet localization performance still degrades. We propose a novel BS-dependent data association and synchronization bias model, integrated into a joint Bayesian framework and inferred via the sum-product algorithm on a factor graph. The impact of joint synchronization and source separation is analyzed under various system configurations. Compared with state-of-the-art cooperative MP-SLAM assuming orthogonal and synchronized BSs, our statistical analysis shows no significant performance degradation. The proposed BS-dependent data association model constitutes a principled approach for classifying features by arbitrary properties that persist over time, such as reflection order or feature type (scatter points versus walls).

## I. INTRODUCTION

Location awareness is a key ingredient for future 6G communication networks, enabling adaptive beamforming, efficient resource allocation, and interference management in the context of integrated communication and sensing (ISAC) [1], [2]. Yet, radio-based localization of mobile terminals (MTs) remains challenging in indoor and urban environments [3], [4], which are dominated by strong multipath propagation and frequent obstructed line-of-sight conditions (see Fig. 1). These effects can lead to localization outages and, consequently, degrade communication performance in ISAC systems.

In contrast to conventional methods that treat multipath as interference, multipath-based simultaneous localization and mapping (MP-SLAM) exploits it as an additional source of information by modeling specular reflections as virtual anchors (VAs)—the mirror images of base stations (BSs) at reflecting surfaces [3]. The joint estimation of MTs and VAs thus enables accurate and robust localization even in obstructed line-of-sight conditions [5]–[11].

*State of the Art:* MP-SLAM is a feature-based SLAM method [12], where the environment is represented by static map features—namely, BSs and VAs. Since both the number and positions of these features are unknown, MP-SLAM jointly estimates them together with the agent trajectory. The input measurements (such as time-of-arrival (TOA), angle-of-arrival (AOA), angle-of-departure (AOD) of multipath components (MPCs)) are typically obtained from radio signals via parametric channel estimation algorithms [13]–[15]. The probabilistic formulation of MP-SLAM is commonly derived through belief propagation on a factor-graph representation of the SLAM problem [6], leading to scalable algorithms

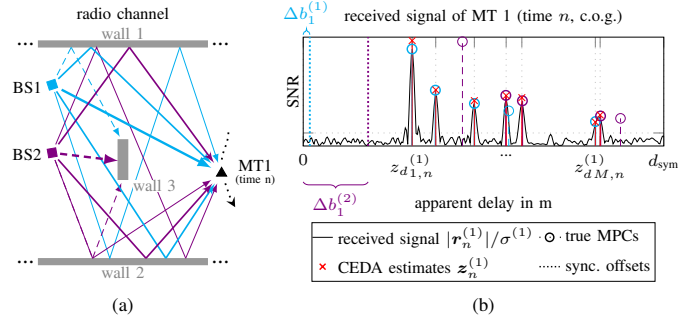


Fig. 1. Figure (a) shows an exemplary environment consisting of three walls including a single MT that receives radio signals via multipath propagation from two *unsynchronized, interfering* BS that transmit using identical frequency bands/symbols. Figure (b) shows the received signal at the center of gravity of MT1 at time  $n$ . The signals from BS1 and BS2 are delayed with respect to time 0 by the apparent synchronization biases  $\Delta b_1^{(1)} = b_{bs,n}^{(1)} - b_{mt,n}^{(1)}$  and  $\Delta b_1^{(2)} = b_{bs,n}^{(2)} - b_{mt,n}^{(1)}$ , which arise from the differences between the corresponding BS and MT clock biases.

suitable for various network scenarios. It has been shown that MP-SLAM constitutes an instance of marginal Poisson multi-Bernoulli (PMB) SLAM, offering an excellent trade-off between estimation robustness and computational scalability compared to other random finite set (RFS)-based SLAM approaches [16]. Recent extensions include cooperative simultaneous localization and tracking (SLAT) [17] and cooperative SLAM within the MP-SLAM framework [18].

When multiple BSs are involved, existing MP-SLAM approaches typically assume perfect clock synchronization among the BSs and orthogonal transmission sequences, such that inter-BS interference at the MT is negligible. A particularly relevant example arises in modern 5G systems, where positioning reference signals (PRS) are used for downlink localization. A major challenge in this context stems from unsynchronized BSs, which transmit signals with irregular timing, thereby causing interference at the MTs [19] (see Fig. 1). Although the PRS standard employs muting patterns to mitigate interference, localization performance and robustness still degrade significantly under such conditions.

*Contributions:* In this work, we present a robust and scalable algorithm for *simultaneous source separation, synchronization, and mapping*. The proposed MP-SLAM algorithm processes downlink radio signals transmitted from multiple unsynchronized BSs to multiple unsynchronized MTs, enabling sequential estimation of multiple moving MTs while jointly detecting and estimating the locations of map features—i.e., BSs and VAs—represented by their PVAs positions and existence probabilities. Since each MT receives a mixture of potentially interfering impulse responses from all visible BSs (see Fig. 1), the algorithm performs probabilistic source separation by associating PVAs to their corresponding BS (cf. Fig. 2). It further conducts probabilistic data association (PDA) between MPCs measurements and PVAs, while jointly

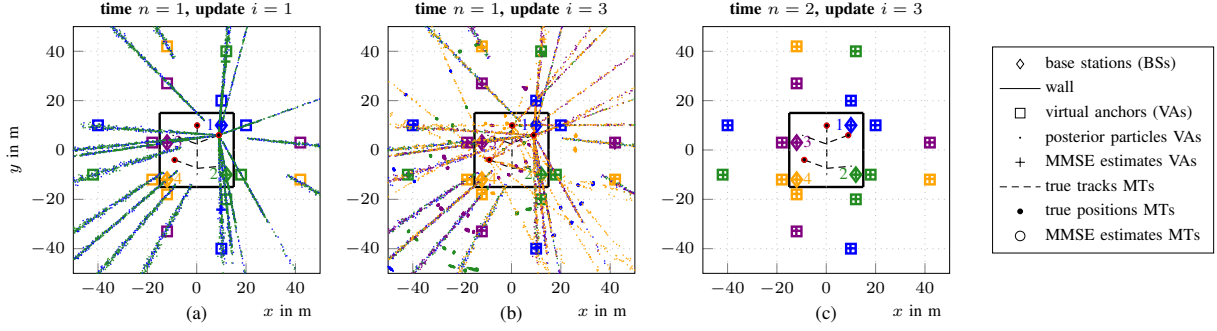


Fig. 2. Simulation environment for time  $n = 1$  after the first MT update (a), the last MT update (b) and for time  $n = 2$  after the last MT update. The colors represent the true (box) and the estimated (+ and dot) association of map features (PVAs) to BSs.

estimating BS-related and MT-related synchronization offsets. This enables consistent data fusion of map features across all unsynchronized and mutually interfering BS–MT communication links. The key contributions are summarized as follows:

- Introduction of a novel data association model for interfering BSs, enabling probabilistic source separation.
- Modeling of apparent synchronization bias as a difference between BS- and MT-related random variables.
- Derivation of the joint posterior distribution and corresponding factor-graph-based sum-product algorithm (SPA) for the complete problem.
- Performance analysis demonstrating the impact of joint synchronization and source separation, and comparison with state-of-the-art cooperative MP-SLAM approaches.

## II. GEOMETRICAL RELATIONS

At time step  $n$ , we consider  $I$  MTs with unknown state  $\mathbf{x}_n^{(i)}$  containing the positions  $\mathbf{p}_n^{(i)} = [p_{x,n}^{(i)} \ p_{y,n}^{(i)}]^T$ , the velocity  $\mathbf{v}_n^{(i)} = [v_{x,n}^{(i)} \ v_{y,n}^{(i)}]^T$ , and antenna array orientation  $o_n^{(i)}$  where  $i \in \{1, \dots, I\}$ . We consider  $J$  BSs with known positions  $\mathbf{p}_{\text{bs}}^{(j)}$ ,  $j \in \{1, \dots, J\}$ . Each BS  $j$  observes  $N_n^{(j)} - 1$  specular reflections of radio signals at flat surfaces, modeled by VAs with known positions  $\mathbf{p}_{\text{va},l}^{(j)} = [p_{x,\text{va},l}^{(j)} \ p_{y,\text{va},l}^{(j)}]^T$ ,  $l \in \{2, \dots, N_n^{(j)}\}$  (see [20]). By applying the image-source model [20], [21], a VA associated with a single-bounce path is the mirror image of  $\mathbf{p}_{\text{bs}}^{(j)}$  at reflective surface  $l$  given by  $\mathbf{p}_{\text{va},l}^{(j)} = \mathbf{p}_{\text{bs}}^{(j)} + 2(\mathbf{u}_l^T \mathbf{e}_l - \mathbf{u}_l^T \mathbf{p}_{\text{bs}}^{(j)}) \mathbf{u}_l$  where  $\mathbf{u}_l$  is the normal vector of reflective surface  $l$ , and  $\mathbf{e}_l$  is an arbitrary point on the considered surface.<sup>1</sup> The according point of reflection  $\mathbf{q}_{l,n}^{(j,i)}$  at the surface is given as

$$\mathbf{q}_{l,n}^{(j,i)} = \mathbf{p}_{\text{va},l}^{(j)} + \frac{(\mathbf{p}_{\text{bs}}^{(j)} - \mathbf{p}_{\text{va},l}^{(j)})^T \mathbf{u}_l}{2(\mathbf{p}_n^{(i)} - \mathbf{p}_{\text{va},l}^{(j)})^T \mathbf{u}_l} (\mathbf{p}_n^{(i)} - \mathbf{p}_{\text{va},l}^{(j)}) \quad (1)$$

and is needed to relate AOD of a specular reflection to the corresponding VA. Both the MTs and all BSs are equipped with antenna arrays. As shown in Fig. 3, the antenna array geometry at the BS is defined by array element positions relative to  $\mathbf{p}_{\text{bs}}^{(j)}$  (with known orientation of zero), and for an MT by positions relative to  $\mathbf{p}_n^{(i)}$  with unknown orientation  $o_n^{(i)}$ . The geometric relationships of the MPC parameters – distance, AOA, and AOD of VA  $k$  for MT  $i$  and BS  $j$  and are given by  $d_{l,n}^{(j,i)} \triangleq \|\mathbf{p}_n^{(i)} - \mathbf{p}_{\text{va},l}^{(j)}\|$ ,  $\varphi_{l,n}^{(j,i)} \triangleq \angle(\mathbf{p}_n^{(i)}, \mathbf{p}_{\text{va},l}^{(j)}) - o_n^{(i)}$  with  $\angle(\mathbf{p}_1, \mathbf{p}_2) = \text{atan2}(p_{y,2} - p_{y,1}, p_{x,2} - p_{x,1})$  and

<sup>1</sup>We consider only VAs associated to single-bounce reflections; extensions to double-bounce reflections can be done in accordance with [20], [22].

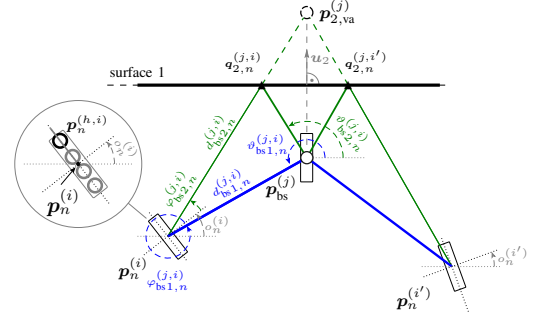


Fig. 3. Exemplary indoor environment with one BS at position  $\mathbf{p}_{\text{bs}}^{(j)}$  and two MTs at position  $\mathbf{p}_n^{(i)}$  and  $\mathbf{p}_n^{(i')}$ , jointly observing a VA at  $\mathbf{p}_{\text{va},l}^{(j)}$ . The figure also illustrates the array geometry of the agents and PAs, assuming  $o_n^{(j)} = 0$ .

$\vartheta_{l,n}^{(j,i)} \triangleq \angle(\mathbf{q}_{l,n}^{(j,i)}, \mathbf{p}_n^{(i)})$ . The according geometric relationships of the line-of-sight (LOS) parameters are given by  $d_{l,n}^{(j,i)} \triangleq \|\mathbf{p}_n^{(i)} - \mathbf{p}_{\text{bs}}^{(j)}\|$ ,  $\varphi_{\text{bs},n}^{(j,i)} \triangleq \angle(\mathbf{p}_n^{(i)}, \mathbf{p}_{\text{bs}}^{(j)}) - o_n^{(i)}$  and  $\vartheta_{\text{bs},n}^{(j,i)} \triangleq \angle(\mathbf{p}_{\text{bs}}^{(j)}, \mathbf{p}_n^{(i)}) - o_{\text{bs}}^{(j)}$ , where  $o_{\text{bs}}^{(j)}$  is known (see Fig. 3).

## III. RADIO SIGNAL MODEL AND CHANNEL ESTIMATION

Each BS  $j$  continuously transmits an radio frequency (RF) pilot signal  $s(t)$  of bandwidth  $B$  at center frequency  $f_c$ . Each MT  $i$  acts as a receiver, observing both, the LOS component and MPCs caused by reflections from surrounding objects. Since all BSs employ the same pilot sequence, every MT observes an inseparable superposition of signals from all BSs.

We consider a MIMO system in which each MT  $i$  and each BS  $j$  is equipped with an antenna array comprising  $H$  and  $H'$  elements, respectively. The array elements are located at positions  $\mathbf{p}_n^{(h,i)} \in \mathbb{R}^2$  for the MT (or  $\mathbf{p}^{(h,j)} \in \mathbb{R}^2$  for the BS), with  $h \in \{1, \dots, H\}$  (or  $h \in \{1, \dots, H'\}$ ), as illustrated in Fig. 3. The array center of gravity is given by  $\mathbf{p}_n^{(i)} = \frac{1}{H} \sum_{h=1}^H \mathbf{p}_n^{(h,i)}$  for the MT (or  $\mathbf{p}_{\text{bs}}^{(j)}$  for the BS). The array orientation of MT  $i$  at time  $n$  is denoted by  $o_n^{(i)}$ , while, without loss of generality, the orientation of each BS is fixed to  $o_{\text{bs}}^{(j)} = 0$ . We further assume that BSs and MTs are mutually unsynchronized. In particular, BS  $j$  has a clock bias  $b_{\text{bs},n}^{(j)}$  and MT  $i$  has a clock bias  $b_{\text{mt},n}^{(i)}$ . At each discrete time index  $n$ , the  $I$  MTs sample the received waveform synchronously at rate  $B$ . In frequency domain, this results in  $M = B/\Delta$  samples with frequency spacing  $\Delta$ . The discrete-frequency RF signal model between BS  $j$  and MT  $i$  is given by [14]

$$r_n^{(i)}[\ell, h, h'] = \sum_{j=1}^J \sum_{l=1}^{N_n^{(j,i)}} \alpha_{l,n}^{(j,i)} e^{i2\pi \frac{f_c}{c} d_{l,n}^{(j,i)} \cos(\vartheta_{l,n}^{(j,i)} - \psi_{l,n}^{(j,i)})}$$

$$\begin{aligned} & \times e^{(i2\pi \frac{f_c}{c} d_n^{(i,h')} \cos(\varphi_{l,n}^{(j,i)} - o_{i,n} - \psi_n^{(i,h')}))} \\ & \times s(\tau_{l,n}^{(j,i)})[\ell] + w_n^{(j,i)}[\ell, h, h'] \end{aligned} \quad (2)$$

where  $s(\tau)[\ell] = S^{(j)}(\ell\Delta)e^{(i2\pi\ell\Delta(\tau + b_{bs_n}^{(j)} - b_{mt_n}^{(i)}))}$  with  $b_{bs_n}^{(j)} - b_{mt_n}^{(i)}$  being the observed clock bias.  $N_{bs_n}^{(j,i)}$  is the number of visible path (related to VAs),  $S^{(j)}(f)$  represents the signal spectrum, which is sampled at  $\ell = -(M-1)/2, \dots, (M-1)/2$ ,  $h$  represent the index for BS antennas<sup>2</sup>,  $h'$  represents the index for MT antennas, and  $c$  is the speed-of-light. The quantities  $d_n^{(i,h')}$  and  $\psi_n^{(i,h')}$  (respectively,  $d_n^{(j,h')}$  and  $\psi_n^{(j,h')}$ ) denote the propagation delay and angle associated with the individual antenna element located at position  $\mathbf{p}_n^{(h,i)}$  (respectively,  $\mathbf{p}_n^{(h,j)}$ ) relative to the center of gravity of the corresponding array.  $\tau_{l,n}^{(j,i)}$ ,  $\varphi_{l,n}^{(j,i)}$  and  $\vartheta_{l,n}^{(j,i)}$  denote respectively delay, AOA and AOD of the MPCs. The complex amplitude  $\alpha_{l,n}^{(j,i)} \in \mathbb{C}$  is given by  $\alpha_{l,n}^{(j,i)} = a_{l,n}^{(j,i)} e^{-j2\pi f_c \tau_{l,n}^{(j,i)}} c / (4\pi f_c d_{l,n}^{(j,i)})$  where  $a_{l,n}^{(j,i)} \in \mathbb{C}$  is a reflection coefficient originating from all interactions of the radio signal with the radio equipment and the associated flat surfaces. The last term  $w_n^{(j,i)}[\ell, h]$  aggregates the measurement noise. The according received signal vector is  $\mathbf{r}_n^{(i)} = [\mathbf{r}_n^{(i)T}[1, 1] \cdots \mathbf{r}_n^{(i)T}[H, 1] \mathbf{r}_n^{(i)T}[1, 2] \cdots \mathbf{r}_n^{(i)T}[H, H']]^T \in \mathbb{C}^{MHH'}$ .

#### A. Parametric Channel Estimation: Measurements

At each time step  $n$  for each MT  $i$ , we apply a channel estimation and detection algorithm (CEDA) [13]–[15] to the discrete MIMO signal vectors, yielding MPC parameters estimates  $\mathbf{z}_{m,n}^{(i)} = [z_{d_{m,n}}^{(i)} z_{\theta_{m,n}}^{(i)} z_{\varphi_{m,n}}^{(i)} z_{\vartheta_{m,n}}^{(i)}]^T$ , where  $m \in \mathcal{M}_n^{(i)} \triangleq \{1, \dots, M_n^{(i)}\}$ . Each  $\mathbf{z}_{m,n}^{(i)}$  contains  $z_{d_{m,n}}^{(i)} \in [0, \tau_{\max}]$ ,  $z_{\theta_{m,n}}^{(i)} \in [-\pi, \pi]$ ,  $z_{\varphi_{m,n}}^{(i)} \in [-\pi, \pi]$ , and  $z_{\vartheta_{m,n}}^{(i)} \in [\gamma, \infty)$ , where  $\gamma$  is the detection threshold. The stacked measurement vector  $\mathbf{z}_n^{(i)} = [z_{1,n}^{(i)T} \cdots z_{M_n^{(i)},n}^{(i)T}]^T$  collects all estimates – each being potentially caused by any interfering BSs  $j \in \{1, \dots, J\}$  (or due to a false positive (FP) of the CEDA).

### IV. SYSTEM MODEL

At each time  $n$ , the proposed method infers random variables explicitly denoted in san serif, upright font. Their definitions are in accordance with Sections II and III. The states of the MTs are given by  $\mathbf{x}_n^{(i)} = [\tilde{\mathbf{x}}_n^{(i)T} \mathbf{v}_n^{(i)T} \mathbf{b}_{mt_n}^{(i)}]^T$ , with the sub-state  $\tilde{\mathbf{x}}_n^{(i)T} = [\mathbf{p}_n^{(i)T} \mathbf{o}_n^{(i)T}]^T$ . The BS biases  $\mathbf{b}_{bs_n}^{(j)}$  are collected by  $\mathbf{b}_{bs,n}^{(j)} = [b_{bs,n}^{(1)} \cdots b_{bs,n}^{(J)}]^T$ .

As in [6], [20], [24], we account for the unknown number of VAs by introducing potential virtual anchors (PVAs)  $k \in \mathcal{K}_n \triangleq \{1, \dots, K_n\}$ . The number  $K_n$  of PVAs of *all interfering* BSs  $j \in \{1, \dots, J\}$  is the maximum possible number of actual VAs, i.e., all VAs that produced a measurement so far [6], [20], [24] (where  $K_n$  increases with time  $n$ ). The states of the PVAs

<sup>2</sup>In 5G systems, access to the impulse responses of individual antenna elements is typically unavailable. Instead, beamforming is performed at the BS, and spreading sequences of individual beams are embedded within dedicated resource blocks (RBs). The signal model in (2) can straightforwardly be reformulated in the beam space following [23], allowing for equivalent application of parametric channel estimation according to Section III-A. Note that we assume the spreading sequences corresponding to different beams to be encoded in RBs within the same PRS symbol. If this assumption is dropped, data association must be carried out individually for each beam, since the inter-BS interference pattern then differs across beams.

are given by  $\mathbf{y}_{k,n} = [\mathbf{p}_{va,k}^T r_{k,n}]^T$ . The existence/nonexistence of PVAs  $k$  is modeled by the existence variable  $r_{k,n} \in \{0, 1\}$  in the sense that PVAs exists if  $r_{k,n} = 1$ . Formally, even if PVAs  $k$  is nonexistent, i.e., if  $r_{k,n} = 0$ , its state is considered. The states  $\mathbf{p}_{va,k}$  of nonexistent PVAs are obviously irrelevant. Therefore, all probability density functions (PDFs) defined for PVA states,  $f(\mathbf{y}_{k,n}) = f(\mathbf{p}_{va,k}, r_{k,n})$ , are of the form  $f(\mathbf{p}_{va,k}, 0) = f_{k,n} f_d(\mathbf{p}_{va,k})$ , where  $f_d(\mathbf{p}_{va,k})$  is an arbitrary “dummy PDF” and  $f_{k,n} \in [0, 1]$  is a constant and can be interpreted as the probability of non-existence [6], [24].

#### A. Measurement Model and New PVAs

An existing PVA generates a measurement  $\mathbf{z}_{m,n}^{(i)} \in \{1, \dots, M_n^{(i)}\}$  with detection probability  $p_d$ . The single-measurement likelihood function (LHF)  $f(\mathbf{z}_{bsm,n}^{(i)} | \mathbf{x}_n^{(i)}, \mathbf{p}_{va,k}, b_{bs,n}^{(j)})$  is assumed conditionally independent across the entries of  $\mathbf{z}_{bsm,n}^{(i)}$  and factorizes as

$$\begin{aligned} f(\mathbf{z}_{m,n}^{(i)} | \mathbf{x}_n^{(i)}, \mathbf{p}_{va,k}, b_{bs,n}^{(j)}) &= f(z_{d_{m,n}}^{(i)} | \mathbf{p}_n^{(i)}, \mathbf{p}_{va,k}, b_{bs,n}^{(j)}) \\ &\quad \times f(z_{\varphi_{m,n}}^{(i)} | \tilde{\mathbf{x}}_n^{(i)}, \mathbf{p}_{va,k}) f(z_{\vartheta_{m,n}}^{(i)} | \mathbf{p}_n^{(i)}, \mathbf{p}_{va,k}) \end{aligned} \quad (3)$$

The LHF of distance, AOA, and AOD are Gaussian,  $f_N(x; \mu, \sigma^2)$ , with

$$\begin{aligned} f(z_{d_{m,n}}^{(i)} | \mathbf{p}_n^{(i)}, \mathbf{p}_{va,k}, b_{bs,n}^{(j)}) &= f_N(z_{d_{m,n}}^{(i)} | d_{k,n}^{(k,i)} \\ &\quad - (b_{mt_n}^{(i)} - b_{bs_n}^{(j)}), \sigma_{d_{k,n}}^{(i)2}) \end{aligned} \quad (4)$$

$$f(z_{\varphi_{m,n}}^{(i)} | \tilde{\mathbf{x}}_n^{(i)}, \mathbf{p}_{va,k}) = f_N(z_{\varphi_{m,n}}^{(i)} | \varphi_{k,n}^{(k,i)}, \sigma_{\varphi_{k,n}}^{(k,i)2}) \quad (5)$$

$$f(z_{\vartheta_{m,n}}^{(i)} | \mathbf{p}_n^{(i)}, \mathbf{p}_{va,k}) = f_N(z_{\vartheta_{m,n}}^{(i)} | \vartheta_{k,n}^{(k,i)}, \sigma_{\vartheta_{k,n}}^{(k,i)2}) \quad (6)$$

where the means  $d_{k,n}^{(k,i)}$ ,  $\varphi_{k,n}^{(k,i)}$  and  $\vartheta_{k,n}^{(k,i)}$  are defined in Section II, and the variances, derived from the Fisher information, are  $\sigma_{d_{k,n}}^{(i)2} = c^2 / (8\pi^2 \beta_{bw}^2 z_{um,n}^{(i)2})$ ,  $\sigma_{\varphi_{k,n}}^{(k,i)2} = 1 / (8\pi^2 z_{um,n}^{(i)2} D^2(\varphi_{k,n}^{(k,i)}))$ , and  $\sigma_{\vartheta_{k,n}}^{(k,i)2} = 1 / (8\pi^2 z_{um,n}^{(i)2} D^2(\vartheta_{k,n}^{(k,i)}))$ . Here,  $\beta_{bw}^2$  denotes the mean square bandwidth and  $D^2(\cdot)$  the normalized squared array aperture [22], [25]. Similarly, for the BS-related LHF, we get

$$\begin{aligned} f_{bs}(\mathbf{z}_{m,n}^{(i)} | \mathbf{x}_n^{(i)}, b_{bs,n}^{(j)}) &= f(z_{d_{m,n}}^{(i)} | \mathbf{p}_n^{(i)}, b_{bs,n}^{(j)}) \\ &\quad \times f(z_{\varphi_{m,n}}^{(i)} | \tilde{\mathbf{x}}_n^{(i)}) f(z_{\vartheta_{m,n}}^{(i)} | \mathbf{p}_n^{(i)}) \end{aligned} \quad (7)$$

where within the individual LHF the geometrical relations  $d_{k,n}^{(k,i)}$ ,  $\varphi_{k,n}^{(k,i)}$ , and  $\vartheta_{k,n}^{(k,i)}$  are replaced by  $d_{bs,n}^{(j,i)}$ ,  $\varphi_{bs,n}^{(j,i)}$ , and  $\vartheta_{bs,n}^{(j,i)}$ , respectively.

Detected VAs, i.e., VAs that generated a measurement for the first time, are modeled by a Poisson process with mean  $\mu_n$  and PDF  $f_n(\bar{\mathbf{p}}_{va,m}^{(j,i)} | \mathbf{x}_n^{(i)})$ . Accordingly, newly detected VAs are represented by *new PVA states*  $\bar{\mathbf{y}}_{n,m}^{(j,i)} = [\bar{\mathbf{p}}_{va,m}^{(j,i)T} \bar{r}_m^{(j,i)T}]^T$ ,  $m \in \{1, \dots, M_n^{(i)}\}$ ,  $j \in \{1, \dots, J\}$  in our statistical model. Each new PVA state corresponds to a measurement  $\mathbf{z}_{bsm,n}^{(i)}$ ;  $\bar{r}_{m,n} = 1$  implies that measurement  $\mathbf{z}_{bsm,n}^{(i)}$  was generated by a newly detected VA. *It is also unknown which BS (if any) caused a measurement  $\mathbf{z}_{bsm,n}^{(i)}$ . Thus, for each index  $m$ , a number of  $J$  new PVAs collected by the stacked vector  $\bar{\mathbf{y}}_{m,n}^{(i)} \triangleq [\bar{\mathbf{y}}_{m,n}^{(1,i)T} \cdots \bar{\mathbf{y}}_{m,n}^{(J,i)T}]^T$  are generated. The unknown BS index  $j$  itself is modeled as a discrete random variable  $\bar{j}_{m,n} \in \{1, \dots, J\}$  with uniform prior probability mass function (PMF)  $p(\bar{j}_{m,n}^{(i)}) \triangleq 1/J$ . However, a new PVA can only correspond to one BS resulting in the PDF*

$$f(\bar{\mathbf{p}}_{va,m}^{(j,i)} | \mathbf{x}_n^{(i)}, \bar{j}_{m,n}^{(i)}) = \begin{cases} f_n(\bar{\mathbf{p}}_{va,m}^{(j,i)} | \mathbf{x}_n^{(i)}), & j = \bar{j}_{m,n}^{(i)} \\ 0, & j \neq \bar{j}_{m,n}^{(i)}. \end{cases} \quad (8)$$

FP measurements generated by the CEDA are modeled as a Poisson process with mean  $\mu_{\text{fp}}$  and PDF  $f_{\text{fp}}(\mathbf{z}_{m,n}^{(i)}) = f_{\text{fp}}(\mathbf{z}_{d,m,n}^{(i)})f_{\text{fp}}(\mathbf{z}_{\varphi,m,n}^{(i)})f_{\text{fp}}(\mathbf{z}_{\theta,m,n}^{(i)})$ , where the individual FP LHF's are uniformly distributed over  $[0, d_{\text{max}}]$ ,  $[-\pi, \pi)$ , and  $[-\pi, \pi)$ , respectively. We denote by  $\bar{\mathbf{y}}_n^{(i)} \triangleq [\bar{\mathbf{y}}_{1,n}^{(i)\text{T}} \cdots \bar{\mathbf{y}}_{M_{\text{bs},n}^{(i)}}^{(i)\text{T}}]^{\text{T}}$ , the joint vector of all new PVA states.

### B. Legacy PVAs and Sequential Update

At time  $n$ , measurements are incorporated sequentially across MTs  $i \in \{1, \dots, I\}$ . Previously detected VAs, i.e., VAs that have been detected either at a previous time  $n' < n$  or at the current time  $n$  but at a previous MT  $i' < i$ , are therefore represented by legacy PVA states  $\mathbf{y}_{k,n}^{(i)}$  with  $\mathbf{y}_{k,n}^{(i)} \triangleq \mathbf{y}_{k,n}^{(1)}$ . Additionally, each legacy PVA implicitly carries an index  $j$  that identifies its corresponding BS. It is given by the mapping

$$\underline{j}(k) = (k-1) \bmod J + 1. \quad (9)$$

New PVAs become legacy PVAs when the next measurements, either of the next MT or at the next time instance, are taken into account. In particular, the VA represented by the new VA state  $\bar{\mathbf{y}}_{m',n'}^{(j,i')}$  introduced due to measurement  $m'$  of MT  $i'$  corresponding to BS  $j$  at  $n' \leq n$  is represented by the legacy PVA state  $\mathbf{y}_{k,n}^{(i)} = [\underline{\mathbf{p}}_{\text{va},m}^{(i)\text{T}} \underline{\mathbf{r}}_m^{(i)\text{T}}]^{\text{T}}$  at time  $n$ , i.e.,

$$k = K_{n'-1} + J \sum_{i''=1}^{i'-1} M_n^{(i'')} + j m'. \quad (10)$$

The number of legacy PVA at time  $n$ , when the measurements of the next MT  $i$  are incorporated, is updated according to  $K_n^{(i)} = K_{n-1}^{(i-1)} + J M_n^{(i-1)}$ , where  $K_n^{(1)} = K_{n-1}$ . Here,  $K_n^{(i)}$  is equal to the number of all measurements collected up to time  $n$  and MT  $i-1$ . The vector of all legacy PVA states at time  $n$  and up to MT  $i$  can now be written as  $\underline{\mathbf{y}}_n^{(i)} = [\underline{\mathbf{y}}_n^{(i-1)\text{T}} \bar{\mathbf{y}}_n^{(i-1)\text{T}}]^{\text{T}}$  and the current vector containing all states as  $\mathbf{y}_n^{(i-1)} = [\underline{\mathbf{y}}_n^{(i-1)\text{T}} \bar{\mathbf{y}}_n^{(i-1)\text{T}}]^{\text{T}}$ .

Let us denote by  $\mathbf{y}_n^{(1)} \triangleq [\underline{\mathbf{y}}_{1,n}^{\text{T}} \cdots \underline{\mathbf{y}}_{K_{n-1},n}^{\text{T}}]^{\text{T}}$ , the vector of all legacy PVA states before any measurements at time  $n$  have been incorporated. After the measurements of all MTs  $i \in \{1, \dots, I\}$  have been incorporated at time  $n$ , the total number of PVA states is

$$K_n = K_{n-1} + J \sum_{i=1}^I M_n^{(i)} = K_n^{(I)} + M_n^{(I)} \quad (11)$$

and the vector of all PVA states at time  $n$  is given by  $\mathbf{y}_n = [\underline{\mathbf{y}}_n^{(I)\text{T}} \bar{\mathbf{y}}_n^{(I)\text{T}}]^{\text{T}}$ .

### C. State Evolution

Legacy PVAs states  $\mathbf{y}_{k,n}$  and the MT states  $\mathbf{x}_n^{(i)}$  are assumed to evolve independently across time according to state-transition PDFs  $f(\mathbf{x}_n^{(i)} | \mathbf{x}_{n-1}^{(i)})$ ,  $f(b_{\text{bs},n}^{(j)} | b_{\text{bs},n-1}^{(j)})$ , and  $f(\mathbf{y}_{k,n} | \mathbf{y}_{k,n-1})$ , respectively. In particular, if PVA  $k$  exists at time  $n-1$ , i.e.,  $r_{k,n-1} = 1$ , it either disappears, i.e.,  $\bar{r}_{k,n} = 0$ , or survives, i.e.,  $\bar{r}_{k,n} = 1$ ; in the latter case, it becomes a legacy PVA at time  $n$ . The probability of survival is denoted by  $p_s$ . In case of survival, its position remains unchanged, i.e., the state-transition PDF of the VA positions  $\underline{\mathbf{p}}_{\text{va},k}$  is given by  $f(\underline{\mathbf{p}}_{\text{va},k} | \mathbf{p}_{\text{va},k}) = \delta(\underline{\mathbf{p}}_{\text{va},k} - \mathbf{p}_{\text{va},k})$ . Therefore,  $f(\underline{\mathbf{p}}_{\text{va},k}, \underline{\mathbf{r}}_{k,n} | \mathbf{p}_{\text{va},k}, r_{k,n-1})$  for  $r_{k,n-1} = 1$  is obtained as

$$f(\underline{\mathbf{p}}_{\text{va},k}, \underline{\mathbf{r}}_{k,n} | \mathbf{p}_{\text{va},k}, r_{k,n-1} = 1)$$

$$= \begin{cases} (1-p_s) f_d(\underline{\mathbf{p}}_{\text{va},k}), & r_{k,n} = 0 \\ p_s \delta(\underline{\mathbf{p}}_{\text{va},k} - \mathbf{p}_{\text{va},k}), & r_{k,n} = 1. \end{cases} \quad (12)$$

If VA  $k$  does not exist at time  $n-1$ , i.e.,  $r_{k,n-1} = 0$ , it cannot exist as a legacy PVA at time  $n$  either, thus we get

$$f(\underline{\mathbf{p}}_{\text{va},k}, \underline{\mathbf{r}}_{k,n} | \mathbf{p}_{\text{va},k}, 0) = \begin{cases} f_d(\underline{\mathbf{p}}_{\text{va},k}), & r_{k,n} = 0 \\ 0, & r_{k,n} = 1. \end{cases} \quad (13)$$

To account for the sequential update, we define  $f^{(i)}(\underline{\mathbf{y}}_{k,n}^{(i)} | \mathbf{y}_{k,n}^{(i-1)})$  for  $i \geq 2$  and  $\underline{\mathbf{r}}_{k-1,n} = 1$  as

$$f^{(i)}(\underline{\mathbf{p}}_{\text{va},k}, \underline{\mathbf{r}}_{k,n} | \mathbf{p}_{\text{va},k}^{(i-1)}, 1) = \begin{cases} f_d(\underline{\mathbf{p}}_{\text{va},k}^{(i)}), & r_{k,n}^{(i)} = 0 \\ \delta(\underline{\mathbf{p}}_{\text{va},k}^{(i)} - \mathbf{p}_{\text{va},k}^{(i-1)}), & r_{k,n}^{(i)} = 1 \end{cases} \quad (14)$$

and for  $\underline{\mathbf{r}}_{k-1,n} = 0$

$$f^{(i)}(\underline{\mathbf{p}}_{\text{va},k}, \underline{\mathbf{r}}_{k,n} | \mathbf{p}_{\text{va},k}^{(i-1)}, 0) = \begin{cases} f_d(\underline{\mathbf{p}}_{\text{va},k}^{(i)}), & r_{k,n}^{(i)} = 0 \\ 0, & r_{k,n}^{(i)} = 1. \end{cases} \quad (15)$$

The initial prior PDF at  $n = 0$  are given as  $f(\mathbf{y}_{k,0}^{(i)})$ ,  $k = \{1, \dots, K_0^{(i)}\}$  and  $f(\mathbf{x}_0^{(i)})$ , where  $\mathbf{y}_{k,0}^{(i)}$  typically is an empty vector. All (legacy and new) PVA states and all MT states up to time  $n$  are denoted as  $\mathbf{y}_n = [\mathbf{y}_n^{(1)\text{T}} \cdots \mathbf{y}_n^{(I)\text{T}}]^{\text{T}}$  and  $\mathbf{y}_{0:n} \triangleq [\mathbf{y}_0^{\text{T}} \cdots \mathbf{y}_n^{\text{T}}]^{\text{T}}$  and  $\mathbf{x}_n = [\mathbf{x}_n^{\text{T}} \cdots \mathbf{x}_1^{\text{T}}]^{\text{T}}$  and  $\mathbf{x}_{0:n} = [\mathbf{x}_0^{\text{T}} \cdots \mathbf{x}_n^{\text{T}}]^{\text{T}}$ , respectively. To model the sequential update of the BS biases, we define the factors  $f^{(i)}(b_{\text{bs},n}^{(j,i)} | b_{\text{bs},n}^{(j,i-1)})$  for  $i \geq 2$  as  $f^{(i)}(b_{\text{bs},n}^{(j,i)} | b_{\text{bs},n}^{(j,i-1)}) = \delta(b_{\text{bs},n}^{(j,i)} - b_{\text{bs},n}^{(j,i-1)})$  with  $b_{\text{bs},n}^{(j)} \triangleq b_{\text{bs},n}^{(j,I)}$ . For  $i = 1$ , we use  $f^{(1)}(b_{\text{bs},n}^{(j,1)} | b_{\text{bs},n}^{(j,0)})$  with  $b_{\text{bs},n}^{(j,0)} \triangleq b_{\text{bs},n-1}^{(j)}$ .

### D. Data Association

Data association between measurements and PVAs is described in a redundant formulation by the PVA/PA-oriented association vector  $\underline{\mathbf{a}}_n^{(i)} \triangleq [\underline{\mathbf{a}}_{1,n}^{(i)} \cdots \underline{\mathbf{a}}_{J,n}^{(i)} \underline{\mathbf{a}}_{J+1,n}^{(i)} \cdots \underline{\mathbf{a}}_{J+K_n^{(i)},n}^{(i)}]^{\text{T}}$  and by the measurement-oriented association vector  $\bar{\mathbf{a}}_n^{(i)} \triangleq [\bar{\mathbf{a}}_{1,n}^{(i)} \cdots \bar{\mathbf{a}}_{M_n^{(i)},n}^{(i)}]^{\text{T}}$ . See [6], [18], [24], [26] for details.

## V. FACTOR GRAPH AND SUM-PRODUCT ALGORITHM

1) *Joint Posterior PDF and Factor Graph*: Using Bayes' rule and independence assumptions related to the state-transition PDFs, the prior PDFs, and the likelihood model (for details please see [6], [20], [24]), and for fixed (observed) measurements  $\mathbf{z}_{1:n}$  (the numbers of measurements  $M_n^{(i)}$  are fixed and not random anymore) the joint posterior PDF of  $\mathbf{y}_{0:n}$ ,  $\mathbf{x}_{0:n}$ ,  $\underline{\mathbf{a}}_{1:n}$ , and  $\bar{\mathbf{a}}_{1:n}$ , conditioned on  $\mathbf{z}_{1:n}$  is given by (16), where the individual LHF-related factors are respectively  $q_{\text{BS}}^{(i)}(\mathbf{x}_n^{(i)}, b_{\text{bs},n}^{(j,i)}, \underline{\mathbf{a}}_{j,n}^{(i)}; \mathbf{z}_{\text{bs},n}^{(i)})$ ,  $q(\mathbf{y}_{k,n}^{(i)}, \mathbf{x}_n^{(i)}, b_{\text{bs},n}^{(j(k),i)}, \underline{\mathbf{a}}_{k+J,n}^{(i)}; \mathbf{z}_{\text{bs},n}^{(i)})$  and  $\bar{q}(\bar{\mathbf{y}}_{m,n}^{(i)}, \mathbf{x}_n^{(i)}, b_{\text{bs},n}^{(j(m),i)}, \bar{\mathbf{a}}_{m,n}^{(i)}; \mathbf{z}_{\text{bs},n}^{(i)})$  that will be discussed next.

The *pseudo LHF's* related to BS  $j$  and MT  $i$  are given by

$$q_{\text{BS}}^{(i)}(\mathbf{x}_n^{(i)}, b_{\text{bs},n}^{(j,i)}, \underline{\mathbf{a}}_{j,n}^{(i)}; \mathbf{z}_{\text{bs},n}^{(i)}) \triangleq \begin{cases} p_d f(\mathbf{z}_{\text{bs},n}^{(i)} | \mathbf{x}_n^{(i)}, b_{\text{bs},n}^{(j,i)}), & \underline{\mathbf{a}}_{j,n}^{(i)} = m \\ \mu_{\text{fp}} f_{\text{fp}}(\mathbf{z}_{\text{bs},n}^{(i)}), & \underline{\mathbf{a}}_{j,n}^{(i)} = 0 \\ 1 - p_d, & \underline{\mathbf{a}}_{j,n}^{(i)} = 0 \end{cases} \quad (17)$$

The *pseudo LHF* for legacy PVA  $k$  and MT  $i$  is given by

$$q(\underline{\mathbf{p}}_{k,\text{va}}^{(i)}, \underline{\mathbf{r}}_{k,n}^{(i)} = 1, \mathbf{x}_n^{(i)}, b_{\text{bs},n}^{(j(k),i)}, \underline{\mathbf{a}}_{k+J,n}^{(i)}; \mathbf{z}_{\text{bs},n}^{(i)})$$

$$\begin{aligned}
& f(\mathbf{y}_{0:n}, \mathbf{x}_{0:n}, \mathbf{a}_{1:n}, \bar{\mathbf{a}}_{1:n}, \bar{\mathbf{j}}_{1:n} | \mathbf{z}_{1:n}) \\
& \propto \underbrace{\left( \prod_{i=1}^{N_{\text{MT}}} f(\mathbf{x}_0^{(i)}) \prod_{k=1}^{K_0} f(\mathbf{y}_{k,0}) \right)}_{\text{MT and VA states initial prior PDFs}} \prod_{n'=1}^n \underbrace{\left( \prod_{i=1}^{N_{\text{MT}}} f(\mathbf{x}_{n'}^{(i)} | \mathbf{x}_{n'-1}^{(i)}) \right)}_{\text{MT state prediction}} \underbrace{\left( \prod_{j=1}^J f(b_{\text{bs},n}^{(j,i)} | b_{\text{bs},n}^{(j,i-1)}) \right)}_{\text{Factors and state prediction related to BSs}} \underbrace{\prod_{m'=1}^{M_{n'}^{(j)}} \Psi(\underline{a}_{j,n'}^{(i)}, \bar{a}_{m',n'}^{(i)})}_{\text{Legacy PVA states prediction}} \underbrace{\left( \prod_{k'=1}^{K_{n'-1}} f(\mathbf{y}_{k',n'} | \mathbf{y}_{k',n'-1}) \right)}_{\text{Legacy PVA states prediction}} \\
& \times \underbrace{\left( \prod_{i=2}^{N_{\text{MT}}} \prod_{k=1}^{K_{n'}^{(i)}} f^{(i)}(\mathbf{y}_{k,n'}^{(i)} | \mathbf{y}_{k,n'}^{(i-1)}) \right)}_{\text{Legacy PVA states transition factors}} \prod_{i=1}^{N_{\text{MT}}} \prod_{k=1}^{K_{n'}^{(i)}} \underbrace{\left( \underline{q}(\mathbf{y}_{k,n'}^{(i)}, \mathbf{x}_{n'}^{(i)}, b_{\text{bs},n}^{(j(k),i)}, \underline{a}_{k+J,n}^{(i)}, \mathbf{z}_{\text{bs},n}^{(i)}) \right)}_{\text{Legacy PVA states related factors}} \prod_{m=1}^{M_{\text{bs},n}^{(i)}} \underbrace{\Psi(\underline{a}_{k,n'}^{(i)}, \bar{a}_{m,n'}^{(i)})}_{\text{New PVA states prior PDF and related factors}} \prod_{m=1}^{M_{\text{bs},n}^{(i)}} \bar{q}(\bar{\mathbf{y}}_{m,n}^{(i)}, \mathbf{x}_n^{(i)}, \mathbf{b}_{\text{bs},n}^{(i)}, \bar{j}_{m,n}^{(i)}, \bar{a}_{m,n}^{(i)}; \mathbf{z}_{\text{bs},n}^{(i)})
\end{aligned} \tag{16}$$

$$\triangleq \begin{cases} \frac{p_d f(\mathbf{z}_{\text{bs},m,n}^{(i)} | \mathbf{x}_n^{(i)}, \underline{\mathbf{p}}_{k,\text{va}}^{(i)}, b_{\text{bs},n}^{(j(k),i)})}{\mu_{\text{fp}} f_{\text{fp}}(\mathbf{z}_{\text{bs},m,n}^{(i)})}, & \underline{a}_{k+J,n}^{(i)} = m \\ 1 - p_d, & \underline{a}_{k+J,n}^{(i)} = 0 \end{cases} \tag{18}$$

and  $\underline{q}(\mathbf{x}_{k,n}^{(i)}, \mathbf{r}_{k,n}^{(i)} = 0, \mathbf{x}_n^{(i)}, b_{\text{bs},n}^{(j(k),i)}, \underline{a}_{k+J,n}^{(i)}; \mathbf{z}_{\text{bs},n}^{(i)}) \triangleq \delta_{\underline{a}_{k,n}^{(i)}}.$

The *pseudo LHF* for new PVA  $m$  and MT  $i$  is given by

$$\bar{q}(\bar{\mathbf{y}}_{m,n}^{(i)}, \mathbf{x}_n^{(i)}, \mathbf{b}_{\text{bs},n}^{(i)}, \bar{j}_{m,n}^{(i)}, \bar{a}_{m,n}^{(i)}; \mathbf{z}_{\text{bs},n}^{(i)}) \triangleq \begin{cases} 0, & j \neq \bar{j}_{m,n}^{(i)} \\ \bar{q}(\bar{\mathbf{y}}_{m,n}^{(i)}, \mathbf{x}_n^{(i)}, \mathbf{b}_{\text{bs},n}^{(j,i)}, \bar{a}_{m,n}^{(i)}; \mathbf{z}_{\text{bs},n}^{(i)}), & j = \bar{j}_{m,n}^{(i)} \end{cases} \tag{19}$$

with

$$\bar{q}(\bar{\mathbf{p}}_{\text{va},m}^{(j,i)}, \bar{\mathbf{r}}_{m,n}^{(j,i)} = 1, \mathbf{x}_n^{(i)}, b_{\text{bs},n}^{(j,i)}, \bar{a}_{m,n}^{(i)}; \mathbf{z}_{\text{bs},n}^{(i)}) \triangleq \begin{cases} 0, & \bar{a}_{m,n}^{(i)} = k \\ \frac{\mu_n f_n(\bar{\mathbf{p}}_{\text{va},m}^{(j,i)} | \mathbf{x}_n^{(i)}) f(\mathbf{z}_{\text{bs},m,n}^{(i)} | \mathbf{x}_n^{(i)}, \bar{\mathbf{p}}_{\text{va},m}^{(j,i)}, b_{\text{bs},n}^{(j,i)})}{J \mu_{\text{fp}} f_{\text{fp}}(\mathbf{z}_{\text{bs},m,n}^{(i)})}, & \bar{a}_{m,n}^{(i)} = 0 \end{cases} \tag{20}$$

and  $\bar{q}(\bar{\mathbf{p}}_{\text{va},m}^{(j,i)}, \bar{\mathbf{r}}_{m,n}^{(j,i)} = 0, \mathbf{x}_n^{(i)}, b_{\text{bs},n}^{(j,i)}, \bar{a}_{m,n}^{(i)}; \mathbf{z}_{\text{bs},n}^{(i)}) \triangleq f_d(\bar{\mathbf{p}}_{\text{va},m}^{(j,i)})$ , respectively. Finally, the binary *indicator functions* that check consistency for any pair  $(\underline{a}_{k,n}^{(i)}, \bar{a}_{m,n}^{(i)})$  of PVA/PA-oriented and measurement-oriented association variable at time  $n$ , read

$$\Psi(\underline{a}_{k,n}^{(i)}, \bar{a}_{m,n}^{(i)}) \triangleq \begin{cases} 0, & \underline{a}_{k,n}^{(i)} = m, \bar{a}_{m,n}^{(i)} \neq k \text{ or } \underline{a}_{k,n}^{(i)} \neq m, \bar{a}_{m,n}^{(i)} = k \\ 1, & \text{otherwise.} \end{cases} \tag{21}$$

The factor graph equivalently representing factorization (16) is shown in Fig. 4.

2) *Confirmation of PVAs and State Estimation:* We estimate the MT states  $\mathbf{x}_n^{(i)}$  (including  $\mathbf{b}_{\text{mt},n}^{(i)}$ ), the BS biases  $\mathbf{b}_{\text{bs},n}^{(i)}$ , and the PVA states  $\mathbf{p}_{\text{va},k}$  from all measurements  $\mathbf{z}_{1:n}$  up to time  $n$  using the respective minimum mean-square error (MMSE) estimates [27, Ch. 4]  $\hat{\mathbf{x}}_n^{(i)} = [\hat{\mathbf{x}}_n^{(i)} \hat{\mathbf{v}}_n^{(i)} \hat{\mathbf{b}}_{\text{mt},n}^{(i)}]$  and  $\hat{b}_{\text{bs},n}^{(j)}$ , which are calculated by the expected values of the respective marginal posterior distributions  $f(\mathbf{x}_n^{(i)} | \mathbf{z}_{1:n})$ ,  $f(b_{\text{bs},n}^{(j)} | \mathbf{z}_{1:n})$ . Detection of the PVAs  $k \in \{1, \dots, K_n\}$  relies on the posterior existence probabilities  $p(r_{k,n} = 1 | \mathbf{z}_{1:n}) = \int f(\mathbf{p}_{\text{va},k}, r_{k,n} = 1 | \mathbf{z}_{1:n}) d\mathbf{p}_{\text{va},k}$  and the conditional posteriors  $f(\mathbf{p}_{\text{va},k} | r_{k,n} = 1, \mathbf{z}_{1:n}) = f(\mathbf{p}_{\text{va},k}, r_{k,n} = 1 | \mathbf{z}_{1:n}) / p(r_{k,n} = 1 | \mathbf{z}_{1:n})$ . A PVA is confirmed if  $p(r_{k,n} = 1 | \mathbf{z}_{1:n}) > p_{\text{cf}}$  [28].

Since introducing new PVAs causes  $K_n$  to grow indefinitely, a suboptimal pruning step is applied. A PVAs is pruned if  $p(r_{k,n} = 1 | \mathbf{z}_{1:n}) < p_{\text{pr}}$ , except for  $k = 1$  of each BS, which is always retained. Note that before pruning  $\underline{j}(k)$  needs to be saved, since (9) becomes invalid. For existing PVAs, we determine the MMSE estimate  $\hat{\mathbf{p}}_{\text{va},k}$  by calculating the expected value of  $f(\mathbf{p}_{\text{va},k} | r_{k,n} = 1, \mathbf{z}_{1:n})$ . Since direct marginalization of (16) is intractable, sequential message passing via the SPA on a factor graph [29] provides efficient approximations (“be-

liefs”) of all marginal posteriors  $f(\mathbf{x}_n^{(i)} | \mathbf{z}_{1:n})$ ,  $f(b_{\text{bs},n}^{(j)} | \mathbf{z}_{1:n})$ ,  $f(\mathbf{p}_{\text{va},k} | r_{k,n} = 1, \mathbf{z}_{1:n})$ , and  $p(r_{k,n} | \mathbf{z}_{1:n})$ , for all MT states  $\mathbf{x}_n^{(i)}$ , BS biases  $b_{\text{bs},n}^{(j)}$ , and PVAs  $k$ . The runtime of the proposed algorithm scales linearly in the number of PVAs, measurements, MTs and particles, i.e.  $\mathcal{O}(JK_{n-1}^{(i)} M_n^{(i)} P)$ . The number of PVAs, which increases over time  $n$  and MT index  $i$  according to (11), can become large. Compared to state-of-the-art cooperative MP-SLAM [18] the proposed algorithm involves an additional factor  $J$ , since a new PVA is generated for each anchor. This is counteracted by pruning.

3) *Selected SPA Messages:* A complete derivation of all SPA messages is omitted due to page limitation; only the key messages relevant to new PVAs are presented (see [6], [20]).

a) *Measurement Evaluation for New PVAs:* The messages  $\xi(\bar{a}_{m,n}^{(i)})$  sent from the factor node  $\bar{q}(\bar{\mathbf{y}}_{m,n}^{(i)}, \mathbf{x}_n^{(i)}, \mathbf{b}_{\text{bs},n}^{(i)}, \bar{j}_{m,n}^{(i)}, \bar{a}_{m,n}^{(i)}; \mathbf{z}_{\text{bs},n}^{(i)})$  to the variable nodes corresponding to the measurement-oriented association variables  $\bar{a}_{m,n}^{(i)}$  are given by

$$\xi(\bar{a}_{m,n}^{(i)}) = \sum_{\bar{j}_{m,n}^{(i)}=1}^J \sum_{\bar{\mathbf{r}}_{m,n}^{(j,i)} \in \bar{\mathcal{R}}_{m,n}^{(i)}} \dots \sum \iint \tilde{f}^{(i)}(\mathbf{x}_n^{(i)}) \bar{q}(\bar{\mathbf{p}}_{\text{va},m}^{(i)}, \bar{\mathbf{r}}_{m,n}^{(i)}, \mathbf{x}_n^{(i)}, \mathbf{b}_{\text{bs},n}^{(i)}, \bar{j}_{m,n}^{(i)}, \bar{a}_{m,n}^{(i)}; \mathbf{z}_{\text{bs},n}^{(i)}) d\mathbf{x}_n^{(i)} d\bar{\mathbf{p}}_{\text{va},m}^{(i)} \tag{22}$$

where the new PVA state  $\bar{\mathbf{y}}_{m,n}^{(i)} = [\bar{\mathbf{p}}_{\text{va},m}^{(i)} \bar{\mathbf{r}}_{m,n}^{(i)}]^\top$  is replaced by its entries. Using the expression of  $\bar{q}(\bar{\mathbf{y}}_{m,n}^{(i)}, \mathbf{x}_n^{(i)}, \mathbf{b}_{\text{bs},n}^{(i)}, \bar{j}_{m,n}^{(i)}, \bar{a}_{m,n}^{(i)}; \mathbf{z}_{\text{bs},n}^{(i)})$  in (20), Eq. (22) simplifies to  $\xi(\bar{a}_{m,n}^{(i)}) = 1$  for  $\bar{a}_{m,n}^{(i)} \in \mathcal{K}_n$ , and for  $\bar{a}_{m,n}^{(i)} = 0$  it becomes

$$\xi(\bar{a}_{m,n}^{(i)}) = 1 + \frac{\mu_n}{J \mu_{\text{fp}} f_{\text{fp}}(\mathbf{z}_{\text{bs},n}^{(i)})} \sum_{j=1}^J \iint f_n(\bar{\mathbf{p}}_{\text{va},m}^{(j,i)} | \mathbf{x}_n^{(i)}) \times f(\mathbf{z}_{\text{bs},m,n}^{(i)} | \mathbf{x}_n^{(i)}, \bar{\mathbf{p}}_{\text{va},m}^{(j,i)}, b_{\text{bs},n}^{(j,i)}) \tilde{f}^{(i)}(\mathbf{x}_n^{(i)}) d\mathbf{x}_n^{(i)} d\bar{\mathbf{p}}_{\text{va},m}^{(j,i)}. \tag{23}$$

b) *Measurement Update for New PVAs:* Finally, the messages  $\phi(\bar{\mathbf{y}}_{m,n}^{(j,i)}) \triangleq \phi(\bar{\mathbf{x}}_{m,n}^{(j,i)}, \bar{\mathbf{r}}_{m,n}^{(j,i)})$  sent to each new PVA variable node are obtained as

$$\begin{aligned}
& \phi(\bar{\mathbf{x}}_{m,n}^{(j,i)}, \bar{\mathbf{r}}_{m,n}^{(j,i)}) \\
& = \int \bar{q}(\bar{\mathbf{p}}_{\text{va},m}^{(i)}, \bar{\mathbf{r}}_{m,n}^{(i)}, \bar{a}_{m,n}^{(i)} = 0, \mathbf{x}_n^{(i)}, j_{m,n}^{(i)} = j; \mathbf{z}_{\text{bs},n}^{(i)}) \\
& \quad \times \tilde{f}^{(i)}(\mathbf{x}_n^{(i)}) d\mathbf{x}_n^{(i)} \zeta(\bar{a}_{m,n}^{(i)} = 0) \end{aligned} \tag{24}$$

resulting in

$$\begin{aligned}
\phi(\bar{\mathbf{x}}_{m,n}^{(j,i)}, 1) & = \int \bar{q}_j(\bar{\mathbf{p}}_{\text{va},m}^{(j,i)}, 1, 0, \mathbf{x}_n^{(i)}; \mathbf{z}_{\text{bs},n}^{(i)}) \\
& \quad \times \tilde{f}^{(i)}(\mathbf{x}_n^{(i)}) d\mathbf{x}_n^{(i)} \zeta(\bar{a}_{m,n}^{(j,i)} = 0) \end{aligned} \tag{25}$$

$$\phi(\bar{\mathbf{x}}_{m,n}^{(j,i)}, 0) \triangleq \phi_{m,n}^{(j,i)} = \sum_{\bar{a}_{m,n}^{(i)} \in \mathcal{K}_n^{(i)}} \zeta(\bar{a}_{m,n}^{(i)}). \tag{26}$$

## VI. RESULTS

We consider a simple indoor scenario as shown in Fig. 2. The scenario comprises four BSs and 4 reflective surfaces, i.e., 4 VAs per BS. Three MTs move along tracks which are observed for 400 time instances  $n$  with observation period  $\Delta T = 1$  s. Measurements are generated according to the system model in Section IV. The signal-to-noise-ratio (SNR) is set to 40 dB at a LOS distance of 1 m. The amplitudes of the MPCs (including the LOS component) are calculated using free-space path loss and an additional attenuation of 3 dB for each reflection at a surface. The detection threshold is  $\gamma = 8$  dB and  $p_d = 0.8$ . False positive measurements are generated according to the model in Section III with a mean number of FPs  $\mu_{fp} = 5$ . For the calculation of the measurement variances, we assume a system bandwidth of  $B = 100$  MHz at a center frequency of  $f_c = 6$  GHz. The arrays employed at MTs and PAs are of identical geometry with  $H = H^{(j)} = 4$  antenna elements forming a uniform rectangular array spaced at  $\lambda/2$ , where  $\lambda = c/f_c$  is the carrier wavelength. The true BS biases are equally spread in a range of  $\pm 30$  m ( $\pm 100$  ns), while the MT biases are spread in a small range between  $\pm 0.5$  m and the true delay biases drift over time following a zig-zag pattern with a slope of 0.01 ns. We use  $10^4$  particles. The particles for the initial MT position and velocity are drawn from i.i.d. Gaussian distributions with center being drawn from the same distribution for each realization, which is centered around the true MT state, and initialization standard deviations given as 0.5 m and 0.1 m/s. The initial orientation is determined from the velocity, assuming the agent to move in forward-facing direction. When  $n = 0$ , the number of VAs is 0, i.e., no prior map information is available. The prior for new PVA states  $f_n(\bar{\mathbf{x}}_{m,n}^{(j)}|\mathbf{x}_n)$  is uniform on the square region given by  $[-45 \text{ m}, 45 \text{ m}] \times [-45 \text{ m}, 45 \text{ m}]$  around the center of the floor plan shown in Fig. 2 and the mean number of new PVAs at time  $n$  is  $\mu_n = 0.01$ . As a proposal distribution for the prior we use annulus shaped distributions, centered around the measurement for numerical efficiency. The probability of survival is  $p_s = 0.999$ . The confirmation threshold and the pruning threshold, are given as  $p_{cf} = 0.5$  and  $p_{pr} = 10^{-3}$ , respectively. The BS synchronization biases initialized uniformly distributed between  $-100$  ns and 100 ns and the MT synchronization biases are initialized uniformly distributed between  $-1$  ns and 1 ns. The MT state transition PDF  $f(\mathbf{x}_n|\mathbf{x}_{n-1})$  is modeled independently for MT bias, MT orientation and the MTs position-velocity state  $[\mathbf{p}_n, \mathbf{v}_n]$ . The MT position-velocity state is modeled by a constant-velocity and stochastic-acceleration model [30] with acceleration variances set to  $\sigma_w = 10^{-3} \text{ m/s}^2$ . The orientation state transition is modeled by a Gaussian random walk with standard deviation of  $3^\circ$ . The state transitions of both, the MT biases and the BS biases, are modeled by a Gaussian random walk with driving noise set to  $\sigma_{bBS} = \sigma_{bMT} = 0.1$  ns. The localization and mapping performance is measured in terms of the mean root mean squared error (RMSE) of the MT positions as well as the optimal subpattern assignment (OSPA) error [31] of all VAs with cutoff parameter set to 1 m and order set to 2. The mean OSPA (MOSPA) errors and RMSEs are obtained using 100 simulation runs.

*Experiment:* To investigate the proposed method, we evaluate four algorithm variants: (i) unsynchronized and inter-

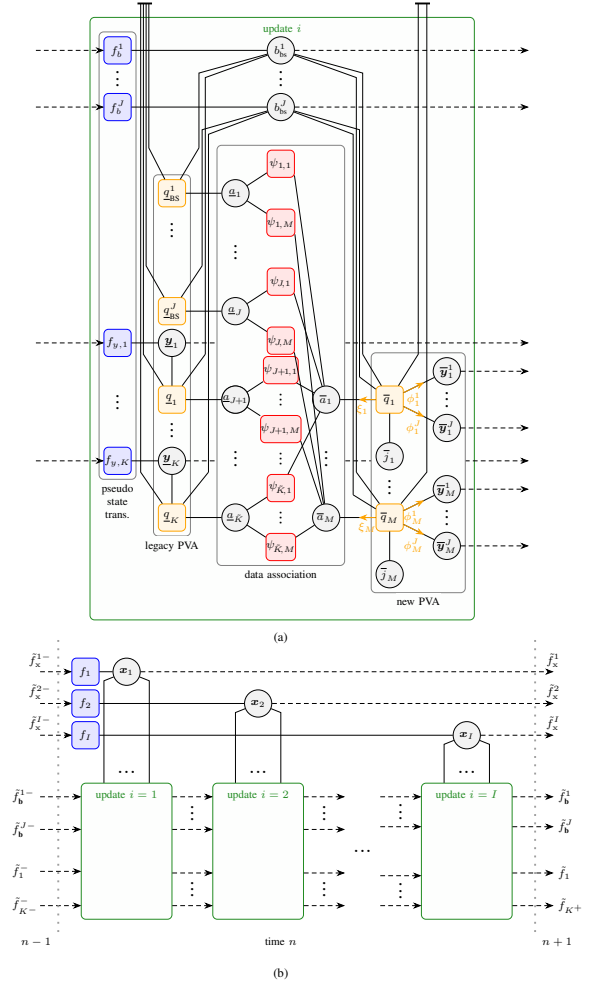


Fig. 4. Factor graph corresponding to the factorization shown in (16). Dashed arrows represent messages that are only passed in one direction. The detailed graph in (a) represents the green subgraphs of the overall factor graph in (b). The following short notation is used. Variables and variable nodes:  $\mathbf{x}_i \triangleq \mathbf{x}_n^{(i)}$ ,  $\mathbf{y}_k^i \triangleq \mathbf{y}_{k,n}^{(i)}$ ,  $\bar{\mathbf{y}}_m^j \triangleq \bar{\mathbf{y}}_{m,n}^{(j,i)}$ ,  $\mathbf{a}_k \triangleq \mathbf{a}_k^{(i)}$ ,  $\bar{\mathbf{a}}_m \triangleq \bar{\mathbf{a}}_m^{(i)}$ ,  $b_{bs}^j \triangleq b_{bs,n}^{(j)}$ ,  $\bar{j}_m \triangleq \bar{j}_{m,n}^{(i)}$ ,  $K^- \triangleq K_{n-1}$ ,  $K \triangleq K_n^{(i)}$ ,  $\bar{K} = J + K_n^{(i)}$ , and  $K^+ \triangleq K_n$ . Factor node:  $f_i \triangleq f(\mathbf{x}_n^{(i)}|\mathbf{x}_{n-1}^{(i)})$ ,  $f_{y,k} \triangleq f(\mathbf{y}_{k,n}|\mathbf{y}_{k,n-1})$  for  $i = 1$ ,  $f_{y,k} \triangleq f(\mathbf{y}_{k,n}^{(i)}|\mathbf{y}_{k,n-1}^{(i-1)})$  for  $i > 1$ ,  $f_b^j \triangleq f(b_{bs,n}^{(j)}|b_{bs,n-1}^{(j,i-1)})$ , and  $\psi_{k,m} \triangleq \Psi(\mathbf{a}_{k,n}^{(i)}|\bar{\mathbf{a}}_{m,n}^{(i)})$ . Messages:  $\bar{f}_x^i \triangleq f(\mathbf{x}_n^{(i)}|\mathbf{z}_{1:n})$ ,  $\bar{f}_b^j \triangleq f(b_{bs,n}^{(j)}|\mathbf{z}_{1:n})$ , and  $\bar{f}_k \triangleq f(\mathbf{y}_{k,n}|\mathbf{z}_{1:n})$ , where  $\mathbf{y}_k$  represents an entry of  $\mathbf{y}_n = [\mathbf{y}_n^{(T)} \bar{\mathbf{y}}_n^{(T)T}]^T$ . The dashed arrows indicate messages representing MT and PVA beliefs of time  $n-1$  and  $n+1$ , which are only propagated forward in time and the minus sign “-” indicates beliefs from the previous time  $n-1$ .

fering BSs, (ii) synchronized and interfering BSs, (iii) unsynchronized and orthogonal BSs, and (iv) synchronized and orthogonal BSs, with the (iv) being the reference case that corresponds to state-of-the-art (SOTA) cooperative MP-SLAM according to [18]. Here, “unsynchronized” refers to unknown delay biases between BSs, while “interfering” indicates that the BSs use identical transmission sequences and, thus, it is unknown which MPC in the received radio signal (and, hence, which PVA) corresponds to which BS. For unsynchronized and interfering BS, Figure 2 shows the true PVAs and MT positions along with their respective MMSE estimates of the proposed algorithm for a single realization. One can obtain that the PVA estimates converge to the true colors, which is possible although there is no prior information about the delay biases since the AOD measurements depend on the (known) BS

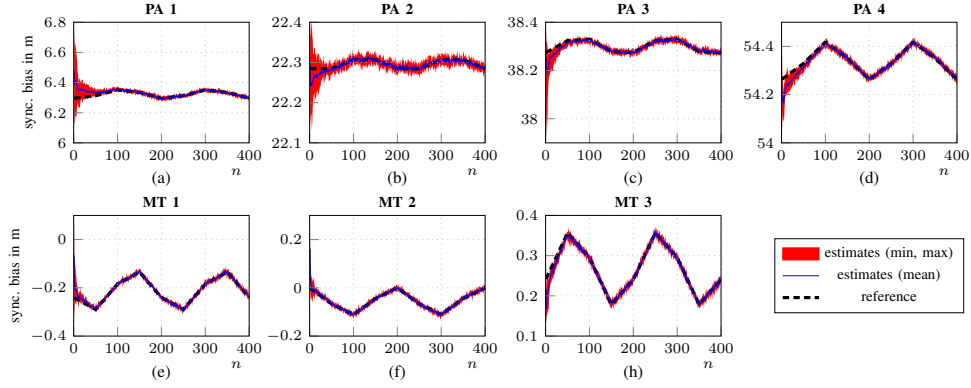


Fig. 5. Performance of MT and BS biases in terms of mean error per time  $n$ .

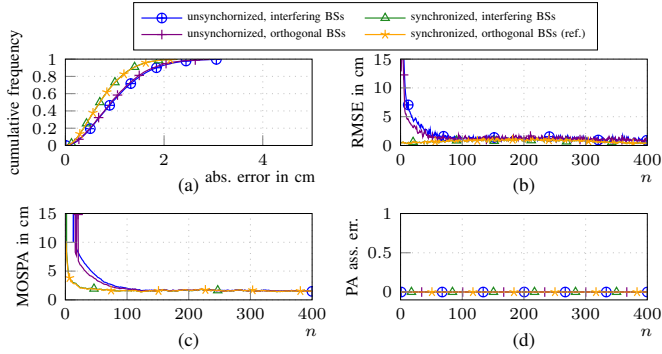


Fig. 6. Performance in terms of (a) the cumulative frequency and (b) average RMSE of the MT position error, (c) PVA MOSPA, and (d) mean number of PA association errors per time  $n$ .

orientation (see Section III). Note that without AOD measurements the proposed algorithm could still differentiate, which VA belongs to which BS, but the colors would be different to the ground truth. The mean RMSE of BS biases and MT biases for  $n \in \{101, \dots, 400\}$  was 26 ps and 24 ps, respectively. The mean error of MT and BS biases are illustrated in Figure 5. Figure 6 provides the numerical results for the experiment in terms of (a) the cumulative frequency and (b) average RMSE of the MT position error, (c) PVA mean optimal subpattern assignment (MOSPA), and (d) mean number of PA association errors per time  $n$ . One can observe that the proposed algorithm takes several times  $n$  to fully converge, leading to an increased MT position error and PVA MOSPA for the first 100 steps  $n$ , but then reaches the performance of the reference algorithm (synchronized, orthogonal BSs). For the investigated setup, there are no PA association errors at any time  $n$  since all detected PAs correspond to the correct BS and thus, there is no significant performance loss for unsynchronized BSs.

## VII. CONCLUSION

This paper presented a Bayesian factor-graph framework for cooperative multipath-based simultaneous localization and mapping (MP-SLAM) with unsynchronized and interfering base stations. The proposed method jointly performs synchronization, source separation, and environment mapping via sequential message passing on a structured sum-product algorithm (SPA). Simulation results show no significant performance degradation of the proposed algorithm compared to state-of-the-art cooperative MP-SLAM that assumes synchronized base stations (BSs) and no inter-BS interference.

The proposed BS-dependent data association model constitutes a principled approach for classifying features by arbitrary properties that persist over time, such as reflection order or feature type (scatter points versus walls). The SPA framework is flexible and can incorporate additional sensing modalities such as IMU or radar, enabling seamless integration into future 6G ISAC systems. Future work will address real-world experiments with 5G PRS data, extensions to dynamic network scenarios or to integrate particle flow to improve the birth of new features through the highly nonlinear models [32], [33].

## REFERENCES

- [1] H. Wymeersch *et al.*, “Joint communication and sensing for 6G - A cross-layer perspective,” in *Proc. IEEE JC&S-2024*, 2024, pp. 1–6.
- [2] N. González-Prelcic *et al.*, “The integrated sensing and communication revolution for 6G: Vision, techniques, and applications,” *Proc. IEEE*, vol. 112, no. 7, pp. 676–723, May 2024.
- [3] K. Witrisal *et al.*, “High-accuracy localization for assisted living: 5G systems will turn multipath channels from foe to friend,” *IEEE Signal Process. Mag.*, vol. 33, no. 2, pp. 59–70, Mar. 2016.
- [4] R. Mendrik, H. Wymeersch, G. Bauch, and Z. Abu-Shaban, “Harnessing NLOS components for position and orientation estimation in 5G millimeter wave MIMO,” *IEEE Trans. Wireless Commun.*, vol. 18, no. 1, pp. 93–107, Jan. 2019.
- [5] C. Gentner *et al.*, “Multipath assisted positioning with simultaneous localization and mapping,” *IEEE Trans. Wireless Commun.*, vol. 15, no. 9, pp. 6104–6117, Sept. 2016.
- [6] E. Leitinger *et al.*, “A belief propagation algorithm for multipath-based SLAM,” *IEEE Trans. Wireless Commun.*, vol. 18, no. 12, Dec. 2019.
- [7] H. Kim *et al.*, “Set-type belief propagation with applications to Poisson multi-Bernoulli SLAM,” *IEEE Trans. Signal Process.*, vol. 72, Apr. 2024.
- [8] A. Venus, E. Leitinger, S. Tertinek, and K. Witrisal, “A graph-based algorithm for robust sequential localization exploiting multipath for obstructed-LOS-bias mitigation,” *IEEE Trans. Wireless Commun.*, vol. 23, no. 2, pp. 1068–1084, June 2023.
- [9] A. Venus, E. Leitinger, S. Tertinek, F. Meyer, and K. Witrisal, “Graph-based simultaneous localization and bias tracking,” *IEEE Trans. Wireless Commun.*, vol. 23, no. 10, pp. 13 141–13 158, May 2024.
- [10] M. Liang, E. Leitinger, and F. Meyer, “Direct multipath-based SLAM,” *IEEE Trans. Signal Process.*, vol. 73, pp. 2336–2352, Mar. 2025.
- [11] Y. Ge, O. Kaltiokallio, Y. Xia, A. F. Garcia-Fernandez, H. Kim, J. Talvitie, M. Valkama, H. Wymeersch, and L. Svensson, “Batch SLAM with PMBM data association sampling and graph-based optimization,” *IEEE Trans. Signal Process.*, vol. 73, pp. 2139–2153, May 2025.
- [12] H. Durrant-Whyte and T. Bailey, “Simultaneous localization and mapping: Part I,” *IEEE Robot. Autom. Mag.*, vol. 13, no. 2, Jun. 2006.
- [13] T. L. Hansen, B. H. Fleury, and B. D. Rao, “Superfast line spectral estimation,” *IEEE Trans. Signal Process.*, vol. PP, no. 99, Feb. 2018.
- [14] S. Grebien, E. Leitinger, K. Witrisal, and B. H. Fleury, “Super-resolution estimation of UWB channels including the dense component – an SBL-inspired approach,” *IEEE Trans. Wireless Commun.*, pp. 1–1, 2024.
- [15] J. Möderl, A. M. Westerkam, A. Venus, and E. Leitinger, “A block-SBL algorithm with dictionary parameter estimation for multi-sensor data fusion,” in *Proc. Fusion-2025*, Brasil, Rio De Janeiro, Jul. 2025.
- [16] H. Kim, K. Granström, L. Svensson, S. Kim, and H. Wymeersch, “PMBM-based SLAM filters in 5G mmWave vehicular networks,” *IEEE Trans. Veh. Technol.*, pp. 1–1, May 2022.

- [17] M. Brambilla *et al.*, “Cooperative localization and multitarget tracking in agent networks with the sum-product algorithm,” *IEEE Open J. of Signal Process.*, vol. 3, pp. 169–195, Mar. 2022.
- [18] E. Leitinger, L. Wielandner, A. Venus, and K. Witrisal, “Multipath-based SLAM for cooperative navigation and map fusion,” in *Proc. Asilomar-24*, Pacific Grove, CA, USA, Oct. 2024.
- [19] S. Hu, A. Berg, X. Li, and F. Rusek, “Improving the performance of OTDOA based positioning in NB-IoT systems,” in *Proc. IEEE GLOBECOM-17*, Jan. 2017, pp. 1–7.
- [20] E. Leitinger, A. Venus, B. Teague, and F. Meyer, “Data fusion for multipath-based SLAM: Combining information from multiple propagation paths,” *IEEE Trans. Signal Process.*, vol. 71, Sep. 2023.
- [21] J. Borish, “Extension of the image model to arbitrary polyhedra,” *JASA*, vol. 75, no. 6, pp. 1827–1836, Mar. 1984.
- [22] X. Li, X. Cai, E. Leitinger, and F. Tufvesson, “A belief propagation algorithm for multipath-based SLAM with multiple map features: A mmWave MIMO application,” in *Proc. IEEE ICC 2024*, June 2024.
- [23] G. Xu, S. Silverstein, R. Roy, and T. Kailath, “Beamspace ESPRIT,” *IEEE Trans. Signal Process.*, vol. 42, no. 2, pp. 349–356, 1994.
- [24] F. Meyer *et al.*, “Message passing algorithms for scalable multitarget tracking,” *Proc. IEEE*, vol. 106, no. 2, pp. 221–259, Feb. 2018.
- [25] A. Fascista *et al.*, “Uplink joint positioning and synchronization in cell-free deployments with radio stripes,” in *Proc. IEEE ICC 2023*, Rome, Italy, May 2023.
- [26] J. Williams and R. Lau, “Approximate evaluation of marginal association probabilities with belief propagation,” *IEEE Trans. Aerosp. Electron. Syst.*, vol. 50, no. 4, pp. 2942–2959, Oct. 2014.
- [27] S. M. Kay, *Fundamentals of Statistical Signal Processing: Estimation Theory*. Upper Saddle River, NJ, USA: Prentice Hall, 1993.
- [28] —, *Fundamentals of Statistical Signal Processing: Detection Theory*. Upper Saddle River, NJ, USA: Prentice Hall, 1998.
- [29] F. Kschischang, B. Frey, and H.-A. Loeliger, “Factor graphs and the sum-product algorithm,” *IEEE Trans. Inf. Theory*, vol. 47, no. 2, pp. 498–519, Feb. 2001.
- [30] Y. Bar-Shalom, X. R. Li, and T. Kirubarajan, *Estimation with Applications to Tracking and Navigation: Algorithms and Software for Information Extraction*. Hoboken, NJ: John Wiley and Sons, 2001.
- [31] D. Schuhmacher, B.-T. Vo, and B.-N. Vo, “A consistent metric for performance evaluation of multi-object filters,” *IEEE Trans. Signal Process.*, vol. 56, no. 8, pp. 3447–3457, Aug. 2008.
- [32] L. Wielandner, E. Leitinger, F. Meyer, and K. Witrisal, “Message passing-based 9-D cooperative localization and navigation with embedded particle flow,” *IEEE Trans. Signal Inf. Process. Netw.*, vol. 9, 2023.
- [33] W. Zhang and F. Meyer, “Multisensor multiobject tracking with improved sampling efficiency,” *IEEE Trans. Signal Process.*, vol. 72, pp. 2036–2053, Mar. 2024.